Journal of Electroanalytical Chemistry 996 (2025) 119369

Contents lists available at ScienceDirect

Journal of Electroanalytical Chemistry

journal homepage: www.elsevier.com/locate/jelechem

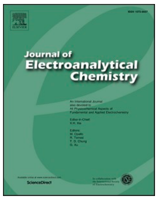

Cost-lowering and performance-improvement of B-γ-$CsSnI_3$ solar cells by adding CZTSSe absorber

Boukhelkhal Feriha Afrah [a], Selmane Naceur [a,*], Cheknane Ali [a,*], Khemloul Fakhereddine [b], Heba Bsharat [c,d], Hikmat S. Hilal [e,*]

[a] Laboratoire Matériaux, Systèmes Énergétiques, Énergies Renouvelables et gestion de l'Énergie (LMSEERGE), Université Amar Telidji de Laghouat, Bd des Martyrs BP37G, Laghouat 03000, Algeria
[b] Laboratoire des Matériaux pour Application et Valorisation des Energies Renouvelables (LMAVER), Université Amar Telidji de Laghouat, Bd des Martyrs BP37G, 03000 Laghouat, Algeria
[c] Department of Physics, An-Najah National University, Nablus, P400, Palestine
[d] Department of Physics, Palestine Technical University (Khadouri), Toulkarm P300, Palestine
[e] SSERL, Department of Chemistry, An-Najah National University, Nablus 400, Palestine

ARTICLE INFO

Keywords:
Bi-absorber solar cell
B-γ-$CsSnI_3$
CZTSSe
Density functional theory (DFT)
SCAPS-1D software

ABSTRACT

Low-cost and environmentally friendly CuZnSnSSe (CZTSSe)-based solar cells suffer low conversion efficiencies. On the other hand, perovskite B-γ-$CsSnI_3$-based cells, may yield higher performance, but still lower than anticipated, and involve the costly cesium. This study aims at lowering the B-γ-$CsSnI_3$ perovskite solar cell costs, without sacrificing performance, by adding a CZTSSe absorbing layer to a thinned perovskite layer. The proposed lead-free cell structure is: ZnO-Al/i-ZnO/CdS/CZTSSe/B-γ-$CsSnI_3$/$MoSe_2$/Mo. This strategy is novel and has not been described for cost lowering in B-γ-$CsSnI_3$ based systems. Density Functional Theory is used to predict the crystalline structure, the electronic and the optical parameters that are in turn used in the SCAPS simulation software. Layer thicknesses are varied for CZTSSe (1–2 μm) and the perovskite (0.1–2 μm), while the doping concentrations are varied from 1×10^{15} to 1×10^{19} cm^{-3}. With doping concentration 1×10^{17} cm^{-3}, the bi-absorber cell exhibits high efficiency of 23.80 % at 0.1 μm perovskite thickness. At thickness 1.0 μm, the efficiency is 29.20 %. These values are higher than literature B-γ-$CsSnI_3$ mono-absorber layer cells of similar thicknesses. The results highlight the added value of CZTSSe layer inclusion, in costly solar cells, while exhibiting higher efficiency.

1. Introduction

Population growth and industrial development have contributed to an increase in global energy demand. With this growth, research shifted to renewable energies as sustainable sources. Among these renewables, solar energy is a widespread free and green energy source. However, the current research trends employed to harvest solar energy still need more to do. Researchers use photovoltaic technology based on absorbers (CIS), (CIGS) and CdTe, but they suffer from limitations such as toxicity, non-abundance and cost. More eco-friendly solar cell materials are needed. One such material is $Cu_2ZnSn(S,Se)_4$ (CZTSSe) [1], where the hazardous indium is replaced with Zn, and the scarce gallium by Sn. CZTSSe comes with additional outstanding properties including the direct band gap that is tunable in the range 1–1.5 eV [2–5] with the high absorption coefficient ($>10^4$ cm^{-1}) [6–8]. Research must take advantage of all of these characteristics and utilize them in higher solar cell performance. Despite these features, CZTSSe cells exhibit power conversion efficiencies no higher than 20 % in single-junction configurations [9–12]. Recently, Hafaifa et al. [13] improved ZnO/CdS/CZTSSe cells efficiency from ∼13 % to ∼18 % by optimizing layer thicknesses and doping concentrations. Therefore, there is room for maneuvering in the CZTSSe research.

Perovskite solar cells include inorganic-organic hybrids or tin halide-based materials, as active layers to harvest light. The cells received considerable attention for their high efficiencies, low production costs, and flexibility in terms of material composition and manufacturing processes [14]. Lead-based perovskite materials with high performance were reported [15], but the presence of the hazardous lead is a

---

* Corresponding authors.
E-mail addresses: n.selmane@lagh-univ.dz (S. Naceur), a.cheknane@lagh-univ.dz (C. Ali), hshilal@najah.edu (H.S. Hilal).

https://doi.org/10.1016/j.jelechem.2025.119369
Received 23 June 2025; Received in revised form 17 July 2025; Accepted 26 July 2025

Table 1
Lattice parameters for CZTSSe and B-γ-$CsSnI_3$ before and after optimization.

	CZTSSe			B-γ-$CsSnI_3$		
	Before optimization	After optimization	Exp [34]	Before Optimization	After optimization	Exp [33]
a (Å)	5.465925	5.475169	5.43	8.677776	8.928713	8.688
b (Å)	5.465925	5.475169	5.43	12.623894	12.516599	12.378
c (Å)	10.910650	10.928220	10.85	8.729731	8.705584	8.643
cell volume (A*3)	325.970247	327.594927		956.318709	972.911087	

limitation. Among perovskite materials is $CsSnI_3$ [16]. Unlike organic perovskites, this inorganic material is soundly stable [17]. Despite that, the oxidation of Sn^{2+} ions to Sn^{4+} is still an issue in this material [18]. Using solid additive-assisted chemical vapor deposition (SACVD) technique effectively suppressed Sn^{2+} oxidation to Sn^{4+}, reduced defect density and enhanced $CsSnI_3$ chemical and optical stabilities. This shows a horizon to improve the perovskite stability [19]. Other methods were also proposed to stabilize the perovskite in literature [20]. Thus, the stability issue can possibly be solved out. Being lead-free, the material is ecofriendly and is not restricted in solar cell applications [21]. $CsSnI_3$ exists in several crystalline phases that vary according to external conditions and temperature. These include: Cubic phase (α-$CsSnI_3$) with Space group Pm3¯m, observed at high temperatures [14,15], tetragonal phase (β-$CsSnI_3$) that is an intermediate phase between cubic and orthorhombic [22], and orthorhombic phase (B-γ-$CsSnI_3$) with space group P-n-m-a, observed at room temperature [22] that is more stable under natural conditions. The material is a direct band p-type semiconductor [23]. Despite the advantages of $CsSnI_3$ materials, they still involve the high-cost cesium constituent. The common wisdom is therefore, to benefit from the advantages of these materials while minimizing the production cost, without compromising performance. Typically, mono-absorber B-γ-$CsSnI_3$ perovskite cells exhibited conversion efficiencies in the range 15–18 %, higher than those of CZTSSe [24]. This is a good feature to start with.

The present cell structure furnishes a strategy to use the B-γ-$CsSnI_3$ perovskite features at lower production cost. Combining the low-cost CZTSSe layer with B-γ-$CsSnI_3$ layer together, is one way out, based on the following assumptions. Firstly, both materials are ecofriendly, which rules out any negative impacts on the environment. Secondly, by minimizing the perovskite layer thickness, the total cost should be cut down. Thirdly, using the two materials in a bilayer absorber mode should enable a wider absorption spectrum, since the two materials have different band gaps. The bi-layer absorber cell should yield higher overall cell performance than either layer separately.

The choice for the two materials is not arbitrary. CZTSSe based solar cells are promising with reported efficiency values of in the range 10.5–13.0 % [1,25–27]. On the other hand, B-γ-$CsSnI_3$ exhibited efficiencies of up to 18 % when used as thin layers [24]. Values of ~24 % were reported when using special treatments for the perovskite [28]. Using 1.4 μm B-γ-$CsSnI_3$ layer yields even higher conversion efficiency values [29]. Ti-based B-γ-$CsSnI_3$ solar cells also exhibited an efficiency of ~24 % when using a 1.0 μm thick absorber layer [30]. Low efficiency B-γ-$CsSnI_3/Cs_2Sn/I_6$ (p-n) heterojunction was reported. The short-circuit photocurrent was improved at higher B-γ-$CsSnI_3$ layer thickness [23], which increases the production cost.

In an earlier communication, we have examined a bi-layer absorber of CuInGaSe (CIGS) and CuZnSnSe (CZTSSe) together. In that report, the costly CIGS layer thickness was minimized by adding the other CZTSSe layer. The bi-layer arrangement showed lowered cost with improved performance [31]. The CZTSSe/$CsSnI_3$ bi-layer absorber, proposed here, was not described earlier to our knowledge.

The present study involves two main parts. The first part aims at enhancing the optical and electronic properties of both materials separately, using the density functional theory (DFT). The second part studies the bi-layer absorbers combined together in the proposed cell structure: ZnO-Al/i-ZnO/CdS/CZTSSe/B-γ-$CsSnI_3/MoSe_2$/Mo using the SCAPS-1D simulator. Effects of thickness and doping concentrations in the absorbing layers, on the cell overall performance and stability, are the focal issues.

2. Density functional theory (DFT)

The Density Functional Theory, DFT, is a common method to study various material properties. Recently, there was significant progress both in theory and applications. This theory, along with computer tools and the ability for rapid computing, makes modeling real vehicles close to mimicking reality within acceptable computation times [23–25].

The DFT was subjected to the Perdew-Burke-Ernzerhof, PBE, exchange correlation potential within generalized-gradient approximation (GGA). Additionally, the CASTEP code plane wave total energy pseudopotential approach was applied [32]. Using the 3D atomistic window in Materials Studio, to simulate the structure, a space group representing the CZTSSe I-4 tetragonal structure and P-n-m-a space group with orthorhombic structure [33] were used. Lattice parameters of CZTSSe and B-γ-$CsSnI_3$, before and after optimization, are summarized in Table 1. The position of atoms are represented, Fig. 1(a). Cu atoms exist

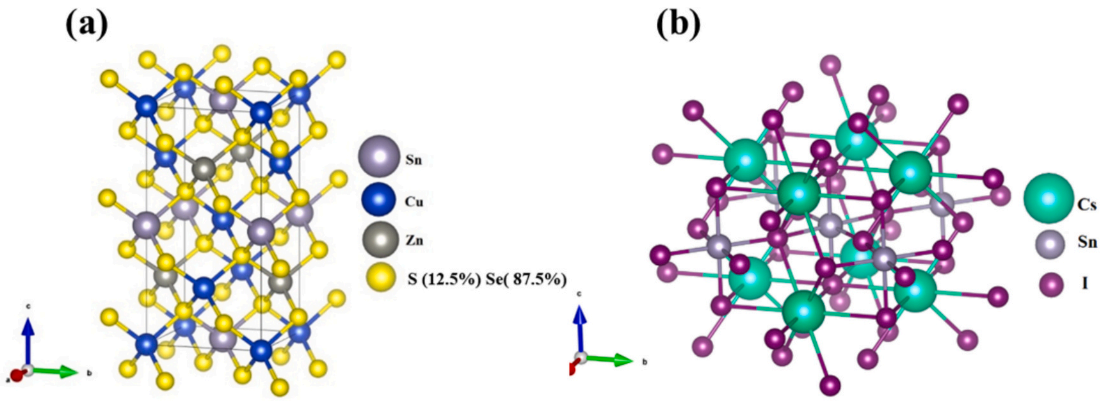

Fig. 1. Crystal structures for the absorber materials (a) CZTSSe and (b) B-γ-$CsSnI_3$.

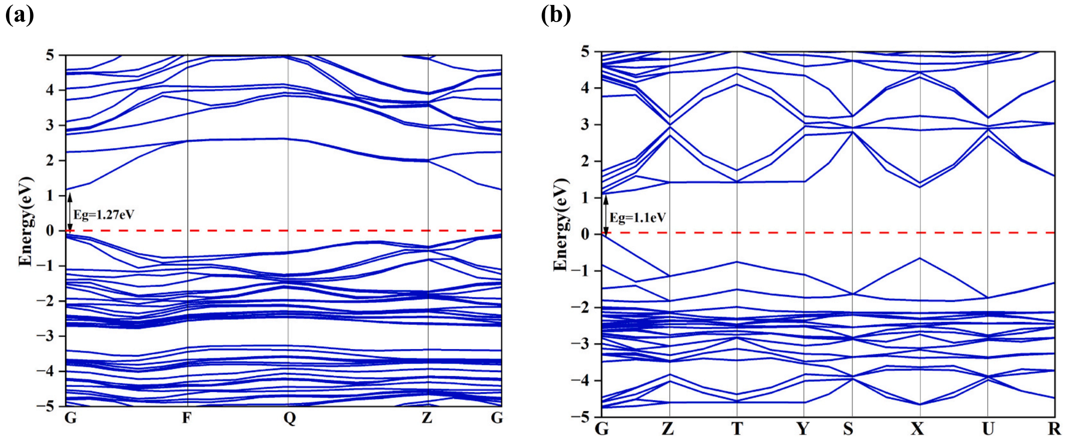

Fig. 2. Band structures for the studied layer materials: (a) CZTSSe and (b) B-γ-CsSnI$_3$

at separate positions, 2a (0.00, 0.00, 0.00) and 2c (0.00, 0.50, 0.25). Zn atoms are at position 2d (0.00, 0.50, 0.75). Sn atoms are placed at 2b (0.00, 0.00, 0.50), while S atoms are at position 8 g (0.75620, 0.24340, 0.12821). The structure Se-doped Cu$_2$ZnSnS$_4$ involves S (12.5 %) and Se (87.5 %).

For B-γ-CsSnI$_3$, Fig. 1(b) shows clearly the cesium (Cs) atom at the position 4c (0.00502, 0.75000, 0.99060), the Sn atom at 4c (0.00, 0.00, 0.50), iodine (I) atoms at separate positions, I$_2$ at 8d (0.20241, 0.00828, 0.79725), and I$_3$ at 4c (0.00041, 0.75000, 0.51981). In order to optimize the present structures, the GGA is used, with the Perdew-Burke-Ernzerhof (PBE) exchange correlation. All of the geometry optimizations and system property computations in this work are carried out using 450 eV cut-off energy and 6 × 6 × 3 of k-points for CZTSSe, and 400 eV, 5 × 3 × 5 for B-γ-CsSnI$_3$.

From Table 1, lattice parameters for CZTSSe are: a = b = 5.465925 Å, c = 10.910650 Å; and for B-γ-CsSnI$_3$ are a = 8.677776 Å, b = 12.623894 Å and c = 8.729731 Å. The structural computations converged once the geometry was optimized, producing the results a = b = 5.475169 Å, c = 10.928220 Å (for CZTSSe) and a = 8.928713 Å, b = 12.516599 Å, c = 8.705584 Å (for B-γ-CsSnI$_3$). The deviations for CZTSSe and B-γ-CsSnI$_3$ are: 0.5 and 1.73 % respectively, and are lower than 5 % for both materials. This implies that the computational techniques and settings employed have excellent accuracy.

3. Electronic and optical property analyses

In this part, the study is focused on simulating crystal structures, optical and electronic properties for each of CZTSSe and B-γ-CsSnI$_3$ materials. The electronic band structure and absorption coefficient are calculated using B3LYP hybrid functionals to further increase the electrical structure calculation accuracy. After that, the obtained results are discussed.

3.1. Electronic properties

Eelectronic properties of a given material underline all the other physical properties of the material. Analyzing and understanding the nature of connections and interactions between the different elements in this material, and then the various phenomena that play a role in defining these physical properties, is thus relevant. Fig. 2 describes the calculated band gap values for the studied materials. Both CZTSSe and B-γ-CsSnI$_3$ materials have direct bandgaps with values 1.27 and 1.10 eV, respectevly, as shown in Figs. 2(a) and (b). Based on Fig. 2, each material has an appropriate band gap to use as as an absorbing layer in solar cells.

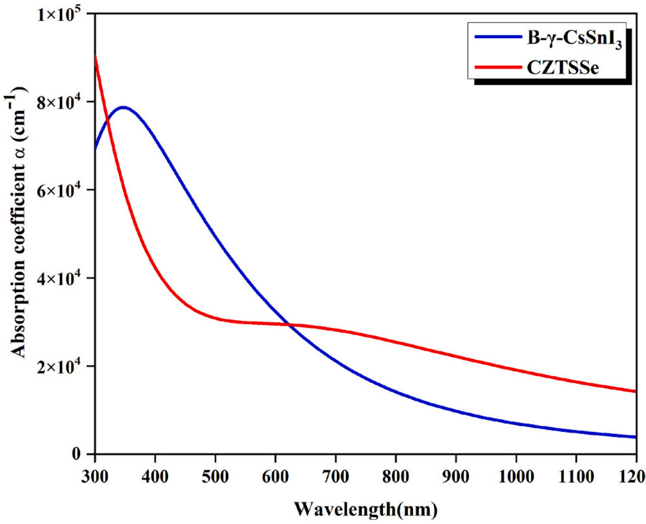

Fig. 3. Absorption coefficient values vs wavelength for (a) CZTSSe material and.

3.2. Optical properties

Absorption coefficient, which is an important parameter to choose the material for photovoltaic applications, is described here. The absorption of radiation by a material is simply explained by the exchange of energy between the atoms of the material and the corpuscles of light. The absorption coefficients for the CZTSSe and B-γ-CsSnI$_3$ perovskite materials are presented in Fig. 3.

(b) B-γ-CsSnI$_3$.

For each of CZTSSe and B-γ-CsSnI$_3$, Fig. 3 presents plots of absorption coefficient vs. wavelength. Both materials exhibit high absorption coefficients, of more than 5 × 10^4 cm^{-1} within the visible, which allows to use them as the absorber layers in the cell.

3.3. SCAPS part

The simulation has been conducted using 3309 version of the numerical SCAPS-1D software, which is a powerful program of heterojunction solar cells. It is based on solving a series of mathematical equations such as: The Poisson, the continuity (eqs. (1) and (2)), transport of electron and hole charge carrier equations (eq. (3)) [35–38].

$$\frac{\partial^2}{\partial x}\varphi(x) = \frac{q}{\varepsilon_0 \varepsilon_r}\left(p(x) - n(x) + N_D + N_A + \rho_P + \rho_n\right) \tag{1}$$

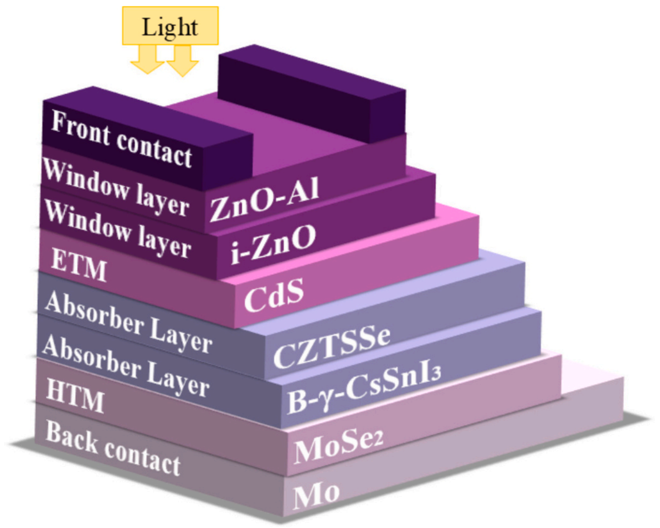

Fig. 4. Schematic structure for the simulated solar cell.

$$\frac{\partial J_P}{\partial x} - R_P + G_P = \frac{\partial P}{\partial x} \tag{2a}$$

$$\frac{\partial J_n}{\partial x} - R_n + G_n = \frac{\partial n}{\partial t} \tag{2b}$$

$$J_n = q\mu_n E_n + qD_n d_n \tag{3a}$$

$$J_P = q\mu_P E_P + qD_P d_P \tag{3b}$$

$$D_P = \frac{KT}{q}\mu_P, D_n = \frac{KT}{q}\mu_n \tag{3c}$$

where φ describes electrostatic potential, ρ is the in-space charge density, E is electric field, $\varepsilon_0$and $\varepsilon_r$are the vacuum and relative permittivity, n & p are free electron and hole concentrations, respectively, N_A and N_D are acceptor & dopant concentrations, μ_n & μ_P describe mobilities of electron and hole, respectively. G_n and G_P are optical generation rates, R_n and R_P are the recombination rates, q represents charge. D_n and D_P are Diffusion coefficients for electrons and holes, K is Boltzmann's constant, and T is temperature (K).

The results obtained provide useful information on solar cell performance. There are many difficulties in solving basic equations in the analytical way, and researchers turn to solving them in numerical ways that require large numbers of repetitions. Researchers have thus developed several solar cell simulators that give accurate results from the most important and widespread SCAPS software [39,40].

To perform a simulation in the SCAPS environment, it is necessary to clearly define the structure to be simulated. A solar cell is made up of a set of thin semiconductor layers. The present solar cell, based on simulated CZTSSe and B-γ-CsSnI$_3$, is ZnO:Al/i-ZnO/CdS/CZTSSe/B-γ-CsSnI$_3$/MoSe$_2$/Mo, (Fig. 4), where ZnO(Al) is the transparent-conducting oxide (TCO) [41] and ZnO is the intrinsic layer. The CdS layer is an n-doped buffer layer having a critical role in cell performance, ensuring the electrical and structural transition between CZTSSe and ZnO. Its presence allows for a considerable reduction in electrical losses associated with recombination mechanisms at the interface [33–35]. CZTSSe and B-γ-CsSnI$_3$ form the bi-layer absorber. MoSe$_2$ functions as the hole-transport material (HTM) which is important because it creates internal capabilities. It creates a strong field within the back-communication area. This minimizes the re-assembly of the carrier and enhances collection and photovoltaic performance [36,37]. Molybdenum (Mo) is the back contact. Layer geometric and physical properties are based on literature, as summarized in Tables 2 and 3.

4. Results and discussions

4.1. Optimized thickness and doping concentration of CZTSSe layer

The effects of thickness and doping concentration of CZTSSe absorbent layer on the ZnO-Al/i-ZnO/CZTSSe/B-γ-CsSnI$_3$/MoSe$_2$/Mo solar cell performance, are first studied, while keeping the perovskite thickness at 0.1 μm and doping concentration at 10^{15} cm^{-3}. The thickness for CZTSSe layer is varied in the range 1–2 μm, with different doping concentrations in the range 1 × 10^{15}–1 × 10^{20} cm^{-3}, based on earlier studies [45]. Fig. 5 summarizes how thickness and doping concentration of CZTSSe layer affect the studied solar cell in terms of (a) short-circuit photocurrent density (J_{SC}), (b) open-circuit potential (V_{OC}), (c) fill-factor (FF%), (d) photo-conversion efficiency (η%) and (e) quantum efficiency (QE%).

Fig. 5 presents the results in the contour forms showing the correlations between thicknesses and doping concentrations of same CZTSSe

Table 3
Parameters of interface defects used in the simulation.

	CdS/CZTSSe	CZTSSe/ B-γ-CsSnI$_3$	B-γ-CsSnI$_3$/ MoSe$_2$
Defects type	neutral	neutral	neutral
Electron-capture cross section, cm^2	1.00E-15	1.00E-15	1.00E-15
Hole-capture cross section, cm^2	1.00E-15	1.00E-15	1.00E-15
Energy distribution	single	single	single
Reference for defect-energy level Et	above highest EV	above highest EV	above highest EV
Energy with respect to Reference eV	0.6	0.6	0.6
Integrated Total density (Over all energies) 1/cm^2	1.00E+8	1.00E+8	1.00E+8

Table 2
Material physical parameters used in simulations.

Parameters	Zno-Al [42]	Zno-i	CdS	B-γ-CsSnI$_3$ [43]	CZTSSe [44]	MoSe$_2$
Layer thickness, μm	0.3	0.05	0.05	0.1	Variable	0.350
Energy band gap (Eg), eV	3.3	3.3	2.4	1.1 DFT	1.27 DFT	1.1
Electronic affinity, eV	4. 4	4.4	4.2	3.620	4.10	4.140
Permittivity (εr)	9.00	9.00	10	48.2	13.6	13.6
Effective density of states (CB) 1/cm^3	1.0E+18	1.0E+18	1.0E+18	1.57E+18	2.2E+18	2.2E+18
Effective density of states (VB),1/cm^3	1.0E+19	1.0E+19	1.0E+19	1.47E+18	1.8E+19	1.8E+19
Thermal velocity electron, cm/s	1.0E+7	1.0E+7	1.0E+7	1.0E+7	1.0E+7	1.0E+7
Thermal velocity of holes, cm/s	1.0E+7	1.0E+7	1.0E+7	1.0E+7	1.0E+7	1.0E+7
Mobility of electrons, cm^2/Vs	1.0E+2	1.0E+2	1.0E+2	4.0E+2	1.0E+2	1.0E+2
Mobility of holes, cm^2/Vs	2.5E+1	2.5E+1	2.5E+1	5.0E+1	2.5E+1	2.5E+1
Donors density (ND), 1/cm^3	1.0E+18	1.0E+17	1.0E+18	0	0	0
Acceptors density (NA), 1/cm^3	0	1.0E+17	0	1.0E+15	Variable	1.00E16

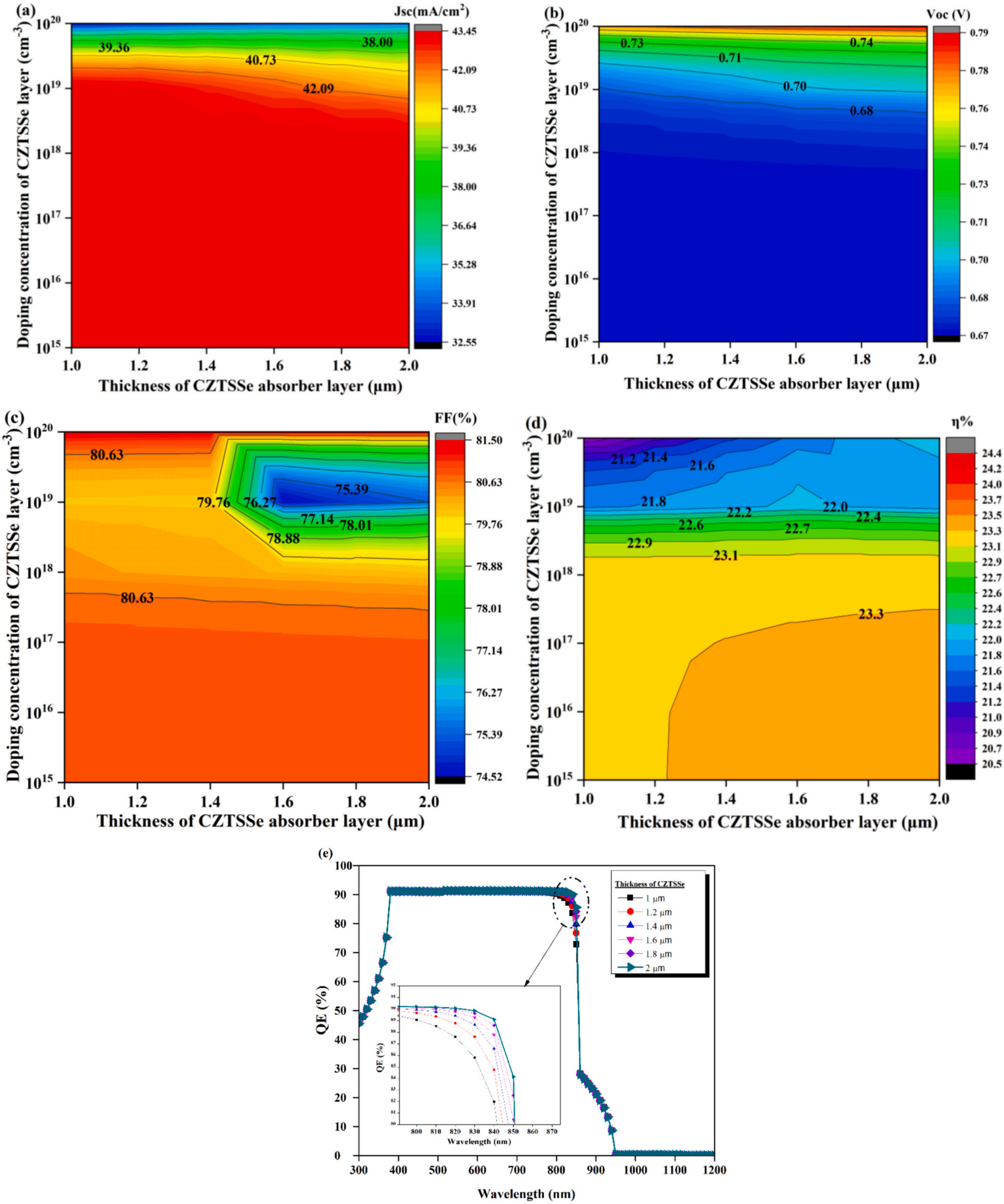

Fig. 5. Effects of CZTSSe layer thickness and doping concentration on the studied solar cell performance.

layer on its characteristics. In Fig. 5(a), the J_{SC} plot color continually changes from blue (lower values) to red (higher values). The J_{SC} values range from 32 mA/cm^2 (blue color) to 43 mA/cm^2 (red color). It also shows that with increasing CZTSSe absorber layer thickness, the current density increases to 43.41 mA/cm^2, while an increase in impurity concentration lowers the value to 32.56 mA/cm^2.

In Fig. 5(b), V_{OC} values continually change from 0.67 V (blue) to 0.79 V (red), passing through the intermediate values (green, yellow,

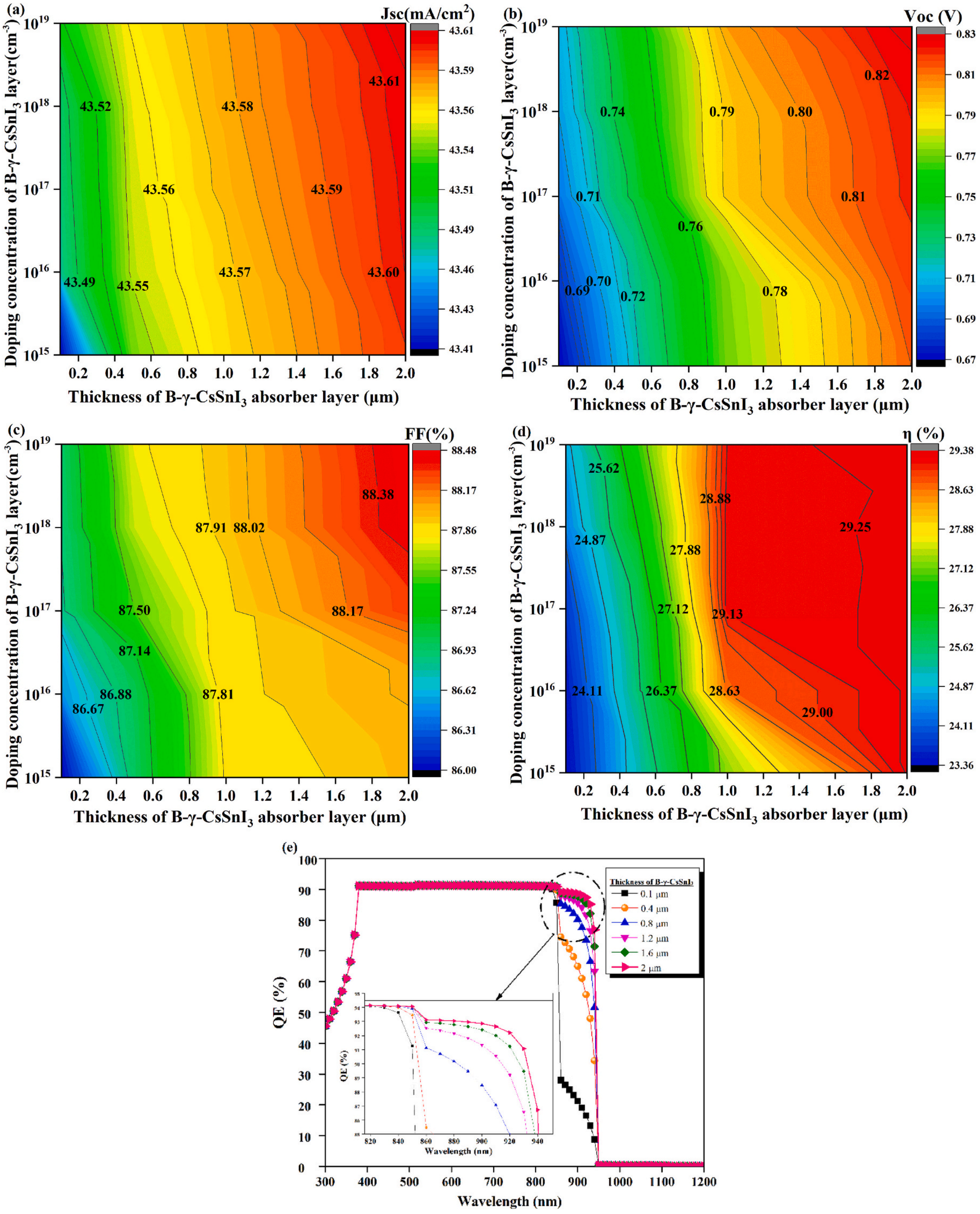

Fig. 6. Effects of B-γ-CsSnI$_3$ layer thickness and doping concentration on the studied cell characteristics.

orange). Fig. 5(c) shows how *FF* value changes. The values continually vary in the range between ~74 % (blue) to 81.50 % (dark red). *FF* values are higher in the orange to red areas, moderate in the green area and lower in the blue area. The highest *FF* (~80.85 %) is achieved at ideal thickness of 2 μm and doping concentration of 1 × 10^{15} cm^{-3}.

Fig. 5(d) describes the efficiency value variation. The highest efficiency (23.36 %) is observed in the yellow region corresponding to a 2 μm thickness and a 1 × 10^{15} cm^{-3} doping concentration. Moving away from this region towards a lower thickness or higher doping levels results in a decrease in efficiency, as evidenced by the transition from yellow to green, then to light blue and finally to dark blue.

With a band gap 1.27 eV, the first absorbing layer (CZTSSe) is responsible for absorbing higher energy photons (with shorter wavelengths) and converting them into charge carriers (electrons and holes). As the first absorbing layer thickness increases, more photons will be absorbed, thereby increasing the cell efficiency to 36 %23.. On the other hand, with increased doping concentration in the same layer, recombination increases between electrons and holes before they move to other electrode terminals. This leads to lower number of charge carriers (electrons and holes), and consequently to lower cell efficiency. For CZTSSe mono-absorber cells, much lower efficiencies of less than 13.0 % are known [1,16,17,27]. The present results thus highlight the bi-

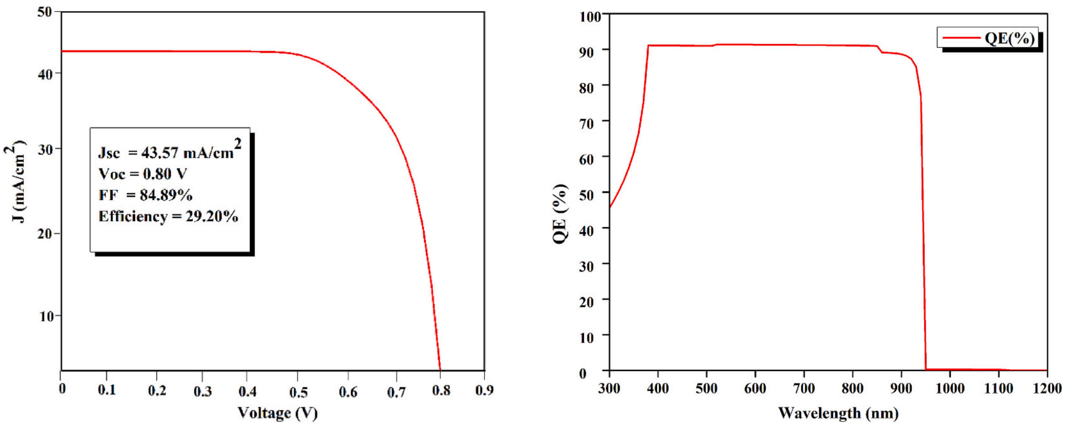

Fig. 7. The Optimal *J-V* characteristics and quantum efficiency for the solar cell at perovskite thickness 1.0 μm.

absorber layer value here.

The results indicate that the optimal thickness and doping concentration are 2 μm and 1 × 10^{15} cm^{-3}, respectively. These parameters yield values of open circuit potential (V_{OC}), short circuit current density (J_{SC}), fill factor (*FF*) and conversion efficiency (η) of 0.67 V, 43.41 mA/cm^2, 86 % and 36 %23., respectively, for the solar cell.

Figure (e) shows that *QE* values. The value increases with increasing CZTSSe layer thickness in the range 1–2 μm within the wavelength range 300 to more than 900 nm, at fixed doping concentration of 1 × 10^{15} cm^{-3}.

4.2. 4.2. Optimized thickness and doping concentration of B-γ-CsSnI$_3$ layer

Using the optimal CZTSSe layer thickness and doping concentration (2 μm and 1 × 10^{15} cm^{-3}, respectively) the thickness and doping concentration of the B-γ-CsSnI$_3$ absorber layer are simulated. Based on earlier reports [46], B-γ-CsSnI$_3$ layer thicknesses are varied in the range 0.1 and 2.0 μm, while its doping concentrations are varied between 1 × 10^{15} and 1 × 10^{20} cm^{-3}. The results are summarized in Fig. 6**.**

Fig. 6 indicates that B-γ-CsSnI$_3$ layer thickness and doping concentration affect the studied solar cell performance. Fig. 6(a) describes how the color scale changes, with layer thickness, from low J_{SC} values (blue), passing through medium values (green and yellow), to higher values (orange), and finally to maximum values (red). Increasing the layer thickness increases J_{SC} to a maximum value of 43.61 mA/cm^2. Conversely, by decreasing the layer thickness and increasing the doping concentration, the current decreases until it reaches the blue area.

Fig. 6(b) shows that at very low doping and thickness values in B-γ-CsSnI$_3$ layer, the V_{OC} is lowered to the blue region. As the doping concentration increases to 1 × 10^{19} cm^{-3}, the V_{OC} value increases, showing a maximum value of 0.83 V.

Fig. 6(c) describes how *FF* changes with layer thickness and doping concentration. The color changes from lower *FF* (blue) to higher value (red) with increased thickness. The highest value 88.48 % is obtained at 2 μm thickness and 1 × 10^{19} cm^{-3} doping concentration.

Fig. 6(d) summarizes the conversion efficiency (η) results. The highest η value is 29.37 % at thickness 2 μm and doping concentration in the range 1 × 10^{15} - 1 × 10^{19} cm^{-3}. The efficiency increases with increased thickness, without lowering in the doping concentration variation within the studied range.

To further confirm these results, the quantum efficiency (*QE*) is studied against B-γ-CsSnI$_3$ layer thickness (from 0.1 to 2.0 μm) within wavelength 300 to more than 900 nm with fixed doping concentration 1 × 10^{19} cm^{-3}. Fig. 6(e) shows that *QE* value increases with increased B-γ-CsSnI$_3$ thickness.

Figs. 6(a) – (c) indicate that J_{SC}, V_{OC} and η increase with increased layer thickness. The results are justified as follows. Very thin absorber layers (<1 μm) physically mean that the depletion region and back contact are too close, which encourages electron capture by this contact. This type of recombination lowers the cell performance by lowering V_{OC}, J_{SC} and consequently η values. At larger thickness of absorber layer (>1 μm), longer wavelength photons may be collected in this layer, which contribute to a higher probability of generating more electron-holes pairs. This increases V_{OC}, J_{SC} and consequently η values.

All-in-all, increasing thickness of each absorber layer to 2 μm improves cell performance. This is due to more light absorption, leading to more electron-hole generations, and consequently higher cell efficiency, reaching a value of 29.37 %. The doping concentration contributed to this result, where it allowed for an increase in the number of generated electrons and holes, or reduced energy loss during the transfer of charge carriers, thereby leading to higher efficiency. Here, the doping concentration works more positively by enhancing absorption and improving charge carrier transport, thus improving the cell efficiency. In addition to the gasket, it helps to create a strong internal electrical field in the dual connection (PN junction) that helps to separate electric carriers (electrons and holes) faster and more efficiently. This increases the electric voltage of the open circuit. On the other hand, it can negatively affect the cell, because at much higher doping concentration excessively increases, the likelihood of recombination increases. Thus, the carriers do not contribute to power generation, which lowers the cell efficiency and the electric voltage of the open circuit. This happens because the internal electric field becomes less effective in separating electric carriers, resulting in reduced voltage.

The results show that as the perovskite layer thickness increases from 1 to 2 μm, only a slight improvement in performance (less than 0.2 %) occurs. Based on this, the optimal cell thickness is 1 μm, with a doping concentration at 1 × 10^{17} cm^{-3}. This choice is to improve efficiency while reducing the cost of raw materials, achieving an ideal balance between performance and cost. Moreover, the results show that lower B-γ-CsSnI$_3$ layer thicknesses may still achieve relatively high efficiencncies. Fig. 6 shows that at perovskite thickness 0.1 μm a high conversion efficiency 23.80 % is achieved. This value is higher than literature B-γ-CsSnI$_3$ mono-absorber layers of comparable thicknesses [24].

The optimal simulated photocurrent density vs potential (*J-V*) characteristics, together with quantum efficiency, for the solar cell are shown in Fig. 7. Table 4 summarizes the present results in comparison with literature values.

Table 4 summarizes the present simulation results in comparison with literature values. Entries 1–4 show that literature CZTSSe thin mono-absorber layers, in both simulation and experimental results, exhibited lower than 15 % efficiency. Upon using low thickness B-γ-CsSnI$_3$ layers here, the efficiency is improved to 23.8 % or higher, entries 17–24.

Table 4
Comparison between solar cell performance with previous studies

a) CZTSSe absorber cell examples

Entry #	Approach	Structure	*Jsc* (mA/cm^2)	*Voc* (V)	*FF* (%)	*η* (%)	Refs.
1	Simulation	ZnO(Al)/ZnO(i)/CdS/ CZTSSe/Mo	27.9	0.81	66.2	14.9	[10]
2	Simulation	ZnO:Al/ i-ZnO/Cds/CZTSSe/Mo	35.2	0.51	69.8	12.6	[9]
3	Exprimental	FTO/ZnO/CdS/CZTSSe/Au	19.5	0.66	65.8	8.4	[11]
4	Exprimental	ZnO:Al/ i-ZnO/Cds/CZTSSe/Mo	32.14	0.45	63.3	9.24	[12]

b) Single B-γ-$CsSnI_3$ absorber layer cell examples

Entry #	Approach	Structure	*Jsc* (mA/cm^2)	*Voc* (V)	*FF* (%)	*η* (%)	Refs.
5	Simulation	Spiro-OMeTAD/ B-γ-$CsSnI_3$/ ZnO/FTO (B-γ-$CsSnI_3$ = 0.2 μm)	25.87	0.95	72.6	17.88	[24]
6	Simulation	Spiro-OMeTAD/ B-γ-$CsSnI_3$/ GaN/FTO (B-γ-$CsSnI_3$ = 0.20 μm)	26.27	0.95	72.2	18.09	[24]
7	Simulation	Spiro-OMeTAD/ B-γ-$CsSnI_3$/ C_{60}/FTO (B-γ-$CsSnI_3$ = 0.15 μm)	20.04	0.96	87.0	16.71	[24]
8	Simulation	Spiro-OMeTAD/ B-γ-$CsSnI_3$/ PCBM/FTO (B-γ-$CsSnI_3$ = 0.200 μm)	20.18	0.95	86.6	16.59	[24]
9	Simulation	Spiro-OMeTAD/ B-γ-$CsSnI_3$/ SnO_2/FTO (B-γ-$CsSnI_3$ = 0.10 μm)	24.16	0.98	65.8	15.5	[24]
10	Simulation	ITO/PCBM/$CsSnI_3$/CFTS/Se (B-γ-$CsSnI_3$ = 1.0 μm)	34	0.87	83	24	[28]
11	Simulation	ITO/NiOx/B-γ-CsSnI3/PCBM/BCP/Al (B-γ-$CsSnI_3$ thickness 1.0 μm)	39.48	0.75	82.3	24	[30]
12	Simulation	CuS/CsSn*I3*/TiO2/ITO (B-γ-$CsSnI_3$ thickness 1.4 μm)	33.5	0.99	87	29	[29]

c) Bi-absorber cell examples

Entry #	Approach	Structure	*Jsc* (mA/cm^2)	*Voc* (V)	*FF* (%)	*η* (%)	Refs.
13	Simulation	ZnO(Al)/ZnO(i)/CdS/ CZTSSe/CIGS/Mo	43.7	0.6036	82.78	21.84	[47]
14	Simulation	Al/AZO/CdS/ ACZTSe/CZTSe (n/p/p +) solar cell	38.99	0.646	73.89	18.63	[48]
15	Simulation	$MAPbI_3$/CdS(nanorods)/ CdS/ACZTSe	42.03	0.786	84.39	27.91	[49]
16	Experimental	Ag/ ITO/ i-ZnO/ CdS/CZTSSe or CAZTSSe/Mo	36.19	0.493	62.86	11.23	[8]

d) ZnO-Al/iZnO/CdS/CZTSSe/B-γ-$CsSnI_3$/MoSe2/Mo bi absorber cells (from this work). CZTSSe thickness = 2 μm, CZTSSe Doping concentration = 10^{15} cm^{-3}, B-γ-$CsSnI_3$ Doping concentration = 10^{17} cm^{-3}

Entry #	B-γ-$CsSnI_3$ thickness	J_{SC} (mA/cm^2)	V_{OC} (V)	*FF* (%)	*η* (%)
17	0.1	43.38	0.68	86.85	23.8
18	0.2	43.49	0.70	87.04	24.19
19	0.4	43.52	0.72	87.39	25.32
20	0.6	43.55	0.75	87.59	26.67
21	0.8	43.56	0.78	87.76	28.7
22	1.0	43.57	0.80	87.89	29.20
23	1.5	43.58	0.81	88.10	29.23
24	2.0	43.61	0.82	88.30	29.37

On the other hand, literature mono-absorber B-γ-$CsSnI_3$ exhibited only low efficiencies of less than 18 % at low thickness, in simulation studies, entries 5–9. With thicker layers, higher efficiency values (24–29 %) were reported by simulation studies, entries 10–12. The present simulated bi-absorber cell with thin B-γ-$CsSnI_3$ layer, 0.1 μm, exhibited efficiencies of ~24% or higher as described in entry 17, which is comparable to the earlier simulated thicker B-γ-$CsSnI_3$ layers, entries 10–12. These results confirm the added value of the CZTSSe layer as a second absorber, where the efficiency is improved at lower B-γ-$CsSnI_3$ thickness and significantly lower production costs.

Entries 13–16 show that literature bi-absorber layers of various simulated or experimental materials exhibited efficiency values lower than the present bi-absorber B-γ-$CsSnI_3$-based systems. The $MAPbI_3$/CdS (nanorods)/CdS/ACZTSe literature simulated cell, entry 15, showed exceptionally high value of ~28 %, but the toxic nature of lead is a serious drawback for this cell.

To further clarify the results, band diagrams are studied for all the layers of the optimized cell, Fig. 8. In the CZTSSe/CdS interface vicinity, the energy bands are bent by varying the electrostatic potential across the p-n junction. The interface CZTSSe/buffer layer exhibits a positive energy discontinuity at the conduction band level of CZTSSe. This discontinuity must have an optimal height for the performance of the

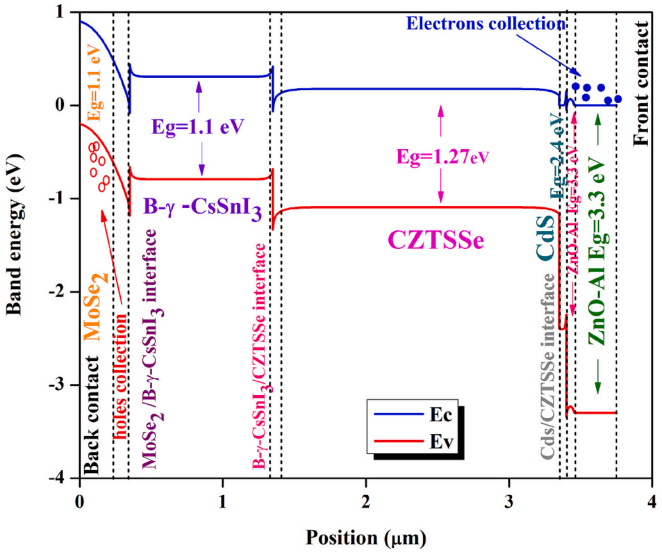

Fig. 8. Band diagram for the proposed solar cell structure.

device. If too high, it opposes the passage of photogenerated electrons, reducing the photocurrent; and if too low (or negative), it increases the dark current and recombination losses. The intrinsic ZnO layer complements the buffer layer, avoiding direct contact with the electrically degenerate ZnO:Al. Due to wide band gaps, the ZnO and buffer layers allow visible radiations to go through [41,50]. The CZTSSe layer, with 1.27 eV band gap, becomes the main absorbing material. It absorbs the penetrating higher energy photons and converts them into electron-hole pairs. The other absorption layer B-γ-$CsSnI_3$, with 1.1 eV band gap, further expands the absorption efficiency and charge generation by absorbing lower energy photons and generating more electron-hole pairs. The $MoSe_2$ layer, placed at the back-contact, behaves as an electrically conductive layer for the back contact, helping to inhibit surface recombination and facilitating the hole transfer towards the back electrode.

All in all, the results indicate that adding a CZTSSe absorber layer to the perovskite B-γ-$CsSnI_3$ layer lowers the production cost while improving the solar cell performance. Other issues with the perovskite, such as its inherent instability to oxidation deserves further study. It is known that the perovskite may undergo Sn^{2+} ion oxidation into Sn^{4+} [51]. Solutions were proposed in earlier literature including coordination with organic materials [24], passivation with Cs_2SnI_6 layers [20], doping [52] or other treatments [18]. In the present study, the added CZTSSe layer may behave as a protective layer for the perovskite layer. This issue has not yet been investigated here, as the study is focused on optimizing layer thickness and doping concentration. However, the protective nature for the CZTSSe layer is worth to further study both experimentally and by simulation.

5. Conclusion

A new lead-free solar cell, involving a bi-absorber layer with CZTSSe and B-γ-$CsSnI_3$ perovskite is proposed. The impact of adding the low-cost and ecofriendly CZTSSe absorber layer on the cell performance is studied, aiming at lowering the cost by using thinner perovskite layer without sacrificing cell performance. The simulation involves two stages: optimizing the optical and electronic properties of the two materials by DFT and then optimizing the bi-layer absorbing cell CZTSSe/B-γ-$CsSnI_3$ performance. Effects of layer thicknesses and doping concentration of each layer are studied. The results confirm the higher performance of the bi-layer absorber layer compared to separate absorbers. Using CZTSSe layer (with thickness 2.0 μm and doping concentration 1×10^{15}) and B-γ-$CsSnI_3$ layer (with doping concentration 1×10^{17} cm^{-3}), the cell exhibits high conversion efficiencies at various perovskite thicknesses. Maximum efficiency of 29.37 % is achieved at 2.0 μm perovskite thickness. At 1.0 μm thickness, the efficiency is only slightly lowered to 29.20 %, which is still higher than earlier reported values for other similar solar cells. Further lowering the perovskite layer thickness to 0.1 μm still yields high efficiency of 23.80 % that is superior to earlier reported values for same perovskite mono-absorber cells. The results confirm the possibility to use B-γ-$CsSnI_3$-based solar cells, with low thickness, for lower cost without sacrificing cell performance, simply by adding CZTSSe as additional absorber.

CRediT authorship contribution statement

Boukhelkhal Feriha Afrah: Writing – original draft, Software, Investigation. **Selmane Naceur:** Writing – review & editing, Validation, Supervision, Conceptualization. **Cheknane Ali:** Writing – review & editing, Supervision, Project administration, Conceptualization. **Khemloul Fakhereddine:** Software. **Heba Bsharat:** Writing – review & editing, Validation. **Hikmat S. Hilal:** Writing – review & editing, Validation.

Declaration of competing interest

The authors declare that they have no known competing financial interests or personal relationships that could have appeared to influence the work reported in this paper.

Acknowledgment

Thanks are due to Professor Marc Burgelman, Gent University-Belgium, for software help. N. Selmane and A. Cheknane thank Amar Telidji University-Laghouat for support (PRFU Project # A10N01UN030120220002, title: Contribution à l'étude des propriétés physico-chimiques des nouveaux matériaux: Applications dans le domaine des énergies renouvelables. They also thank General Directorate of Scientific Research & Technological Development- DGRSDT-, Algeria.

References

[1] L. Wang, R. Liu, H. Luan, Y. Wang, L. Siqin, S. Li, J. Zhang, B. Yao, C. Zhu, The enhancement of CZTSSe solar cell performance through active construction of the double-layer absorber, Solar Energy Materials and Solar Cells 266 (2024) 112670, https://doi.org/10.1016/j.solmat.2023.112670.

[2] X. Zhou, Y. Xue, L. Wang, CZTSSe thin film solar cells with two absorber layers and a PbS layer, J. Phys. Conf. Ser. 2840 (2024) 012010, https://doi.org/10.1088/1742-6596/2840/1/012010.

[3] S. Hong, Investigation of gradient band gap in Cu2ZnSnS4 thin films with residual strain, Curr. Appl. Phys. 58 (2024) 65–73, https://doi.org/10.1016/j.cap.2023.12.005.

[4] J. Guo, L. Wang, L. SiQin, C. Yang, Y. Wang, Y. Wang, S. Li, R. Liu, C. Zhu, H. Luan, CdS(in)/CZTSSe bandgap alignment engineering for performance enhancement of solar cells without ZnO layer, Sol. Energy Mater. Sol. Cells 269 (2024) 112787, https://doi.org/10.1016/j.solmat.2024.112787.

[5] I. Zuñiga, J. Conde, J.C. Tinoco, C. Meza-Avendaño, A. Ashok, F. Ramírez-González, H. Vilchis, Analysis of optical and electrical properties in CZTSSe thin film solar cells through the 2d theoretical modeling, Mater Today Commun 39 (2024) 109124, https://doi.org/10.1016/j.mtcomm.2024.109124.

[6] J. Chen, B. Xu, H. Ma, H. Tong, L. Zou, P. Yang, J. Chu, L. Sun, Y. Chen, Enhanced the performance of CZTSSe solar cells by optimized i:ZnO window layer, Mater. Sci. Semicond. Process. 171 (2024) 107993, https://doi.org/10.1016/j.mssp.2023.107993.

[7] N. Selmane, A. Cheknane, K.M. Gueddouda, F.A. Boukhelkhal, N. Baydogan, M.H. S. Helal, H.S. Hilal, RbGeI3/CuZnSnSSe/CuInGaSe/CdS tandem solar cell with improved performance and lowered cost, J. Mater. Sci. Mater. Electron. 35 (2024) 1109, https://doi.org/10.1007/s10854-024-12889-7.

[8] L. Siqin, C. Yang, J. Guo, Y. Wang, L. Wang, Y. Li, Y. Wang, S. Li, X. Chen, H. Luan, R. Liu, C. Zhu, Achieving 11.23% efficiency in CZTSSe solar cells via defect control and interface contact optimization, Solar Energy 283 (2024) 112913, https://doi.org/10.1016/j.solener.2024.112913.

[9] W. Wang, M.T. Winkler, O. Gunawan, T. Gokmen, T.K. Todorov, Y. Zhu, D.B. Mitzi, Device characteristics of CZTSSe thin-film solar cells with 12.6% efficiency, Adv. Energy Mater. 4 (2014), https://doi.org/10.1002/aenm.201301465.

[10] J. Xu, J. Lin, C. Zhuang, Analysis of the open-circuit voltage of Cu2ZnSn(S, se)4 thin film solar cell, Solar Energy 164 (2018) 231–242, https://doi.org/10.1016/j.solener.2018.02.066.

[11] B. Shin, O. Gunawan, Y. Zhu, N.A. Bojarczuk, S.J. Chey, S. Guha, Thin film solar cell with 8.4% power conversion efficiency using an earth-abundant cu $_2$ ZnSnS $_4$ absorber, Prog. Photovolt. Res. Appl. 21 (2013) 72–76, https://doi.org/10.1002/pip.1174.

[12] M.G. Gang, S.W. Shin, C.W. Hong, K.V. Gurav, J. Gwak, J.H. Yun, J.Y. Lee, J. H. Kim, Sputtering processed highly efficient Cu $_2$ ZnSn(S,Se) $_4$ solar cells by a low-cost, simple, environmentally friendly, and up-scalable strategy, Green Chem. 18 (2016) 700–711, https://doi.org/10.1039/C5GC02417J.

[13] L. Hafaifa, M. Maache, S. Rabhi, Z. Allam, Z.I. Gouchida, Y. Benbouzid, A. Zebeir, R. Adjouz, Enhanced CZTSSe thin-film solar cell efficiency: key parameter analysis, Phys. Status Solidi A 222 (2025), https://doi.org/10.1002/pssa.202400332.

[14] A.S.R. Bati, Y.L. Zhong, P.L. Burn, M.K. Nazeeruddin, P.E. Shaw, M. Batmunkh, Next-generation applications for integrated perovskite solar cells, Commun Mater 4 (2023) 2, https://doi.org/10.1038/s43246-022-00325-4.

[15] C. Yang, W. Hu, J. Liu, C. Han, Q. Gao, A. Mei, Y. Zhou, F. Guo, H. Han, Achievements, challenges, and future prospects for industrialization of perovskite solar cells, Light Sci Appl 13 (2024) 227, https://doi.org/10.1038/s41377-024-01461-x.

[16] S. Rawat, J. Madan, Investigating the Impact of Temperature on the Photovoltaic Properties of CsSnI $_3$ -Based Perovskite Solar Cells, in: 2024 International conference on E-mobility, power control and smart systems (ICEMPS), IEEE (2024) 1–5, https://doi.org/10.1109/ICEMPS60684.2024.10559299.

[17] Md.F. Wahid, Md.S. Rahman, N. Ahmed, A. Al Mamun, Md.N. Howlader, T. Paul, Md.M.R. Tareq, Md.S. Rahman, Md.M. Rahman, Performance enhancement of Lead-free CsSnI $_3$ perovskite solar cell: design and simulation with different Electron transport layers, IEEE, Access 12 (2024) 8296–8312, https://doi.org/10.1109/ACCESS.2024.3352444.

[18] T. Ye, X. Wang, K. Wang, S. Ma, D. Yang, Y. Hou, J. Yoon, K. Wang, S. Priya, Localized Electron Density Engineering for Stabilized B-γ CsSnI $_3$ -Based Perovskite Solar Cells with Efficiencies >10%, ACS Energy Lett. (2021) 1480–1489, https://doi.org/10.1021/acsenergylett.1c00342.

[19] H. Li, C. Ye, Y. Jin, L. Wu, Y. Ma, H. Dong, L.K. Ono, Y. Qi, S.B. Donaev, L. Jiang, Z. Wu, C. Xue, S. Wang, Suppressed defects and improved stability of all-inorganic CsSnI $_3$ films by solid additive-assisted chemical vapor deposition process, Small 21 (2025), https://doi.org/10.1002/smll.202412824.

[20] Z. Zhao, J. Wu, F. Fang, T. Li, Y. Zhou, J. Wang, The mechanism of the stability improvement of the B γ -CsSnI $_3$ perovskite doped with fluorine, Mater Res Express 6 (2019) 125534, https://doi.org/10.1088/2053-1591/ab5dd6.

[21] J. Zhou, Z. Xia, M.S. Molokeev, X. Zhang, D. Peng, Q. Liu, Composition design, optical gap and stability investigations of lead-free halide double perovskite cs $_2$ AgInCl$_6$, J Mater Chem A Mater 5 (2017) 15031–15037, https://doi.org/10.1039/C7TA04690A.

[22] P. Sebastia-Luna, U. Pokharel, B.A.H. Huisman, L.J.A. Koster, F. Palazon, H. J. Bolink, Vacuum-deposited Cesium tin iodide thin films with Tunable thermoelectric properties, ACS Appl Energy Mater 5 (2022) 10216–10223, https://doi.org/10.1021/acsaem.2c01936.

[23] J. Zhang, S. Li, P. Yang, W. Liu, Y. Liao, Enhanced stability of lead-free perovskite heterojunction for photovoltaic applications, J. Mater. Sci. 53 (2018) 4378–4386, https://doi.org/10.1007/s10853-017-1890-z.

[24] S. Lin, B. Zhang, T.-Y. Lü, J.-C. Zheng, H. Pan, H. Chen, C. Lin, X. Li, J. Zhou, Inorganic Lead-free B-γ-CsSnI $_3$ perovskite solar cells using diverse Electron-transporting materials: A simulation study, ACS Omega 6 (2021) 26689–26698, https://doi.org/10.1021/acsomega.1c04096.

[25] S. Gohri, J. Madan, R. Pandey, Enhancing the efficiency of SnS-based solar cells using a GLAD technique and CZTSSe layer, Solid State Commun. 377 (2024) 115380, https://doi.org/10.1016/j.ssc.2023.115380.

[26] D. Ma, M. Li, B. Yao, Y. Li, Z. Ding, J. Zhang, C. Wang, Y. Sun, Y. Liu, Y. Zhu, X. Sun, N. Ding, L. Shi, A high effciency (11.06%) CZTSSe solar cell achieved by combining ag doping in absorber and BxCd1-xs/caztsse heterojunction annealing, Solar Energy Materials and Solar Cells 276 (2024) 113037, https://doi.org/10.1016/j.solmat.2024.113037.

[27] Y. Qi, N. Wei, Y. Li, D. Kou, W. Zhou, Z. Zhou, Y. Meng, S. Yuan, L. Han, S. Wu, Passivating Sn $_{Zn}$ defect and optimizing energy level alignment via organic silicon salt incorporation toward efficient solution-processed CZTSSe solar cells, Adv. Funct. Mater. 34 (2024), https://doi.org/10.1002/adfm.202308333.

[28] M.K. Hossain, M.S. Uddin, G.F.I. Toki, M.K.A. Mohammed, R. Pandey, J. Madan, Md.F. Rahman, Md.R. Islam, S. Bhattarai, H. Bencherif, D.P. Samajdar, M. Amami, D.K. Dwivedi, Achieving above 24% efficiency with non-toxic CsSnI $_3$ perovskite solar cells by harnessing the potential of the absorber and charge transport layers, RSC Adv. 13 (2023) 23514–23537, https://doi.org/10.1039/D3RA02910G.

[29] A. Hosen, S. Rahman, M. Brella, S.R. Al Ahmed, Impact of hole transport layers in inorganic Lead-free B-γ-CsSnI3 perovskite solar cells: A numerical analysis, in: The 1st International Electronic Conference on Processes: Processes System Innovation, MDPI, Basel Switzerland, 2022, p. 41, https://doi.org/10.3390/ECP2022-12611.

[30] S. Ramawat, S. Kukreti, D.J. Sapkota, A. Dixit, Insight into the microband offset and charge transport layer's suitability for an efficient inverted perovskite solar cell: A case study for tin-based B-γ-CsSnI $_3$, Energy Fuel 38 (2024) 9011–9026, https://doi.org/10.1021/acs.energyfuels.4c00763.

[31] N. Selmane, A. Cheknane, F. Khemloul, M.H.S. Helal, H.S. Hilal, Cost-saving and performance-enhancement of CuInGaSe solar cells by adding CuZnSnSe as a second absorber, Solar Energy 234 (2022) 64–80, https://doi.org/10.1016/j.solener.2022.01.072.

[32] S.J. Clark, M.D. Segall, C.J. Pickard, P.J. Hasnip, M.I.J. Probert, K. Refson, M. C. Payne, First principles methods using CASTEP, Z Kristallogr Cryst Mater 220 (2005) 567–570, https://doi.org/10.1524/zkri.220.5.567.65075.

[33] I. Chung, J.-H. Song, J. Im, J. Androulakis, C.D. Malliakas, H. Li, A.J. Freeman, J. T. Kenney, M.G. Kanatzidis, CsSnI $_3$: Semiconductor or Metal? High Electrical Conductivity and Strong Near-Infrared Photoluminescence from a Single Material, High Hole Mobility and Phase-Transitions, J Am Chem Soc 134 (2012) 8579–8587, https://doi.org/10.1021/ja301539s.

[34] M.I. Ziane, D. Ouadjaout, M. Tablaoui, R. Nouri, W. Zermane, A. Djelloul, H. Bennacer, A. Mokrani, M. Hadjab, H. Abid, First-principle computed structural and thermodynamic properties of Cu2ZnSn(SxSe1−x)4 Pentanary solid solution, J. Electron. Mater. 48 (2019) 6991–7002, https://doi.org/10.1007/s11664-019-07496-w.

[35] Z. Yi, W. Wang, R. He, J. Zhu, W. Jiao, Y. Luo, Y. Xu, Y. Wang, Z. Zeng, K. Wei, J. Zhang, S.-W. Tsang, C. Chen, W. Tang, D. Zhao, Achieving a high open-circuit voltage of 1.339 V in 1.77 eV wide-bandgap perovskite solar cells *via* self-assembled monolayers, energy, Environ. Sci. 17 (2024) 202–209, https://doi.org/10.1039/D3EE02839A.

[36] C. Kennedy, J. Steinberger, B. Gasson, Y. Hansen, T. Hillman, M. Havránek, D. Pataki, A. Phdungsilp, A. Ramaswami, G.V. Mendez, Greenhouse gas emissions from global cities, Environ. Sci. Technol. 43 (2009) 7297–7302, https://doi.org/10.1021/es900213p.

[37] A.M. Omer, Energy, environment and sustainable development, Renew. Sustain. Energy Rev. 12 (2008) 2265–2300, https://doi.org/10.1016/j.rser.2007.05.001.

[38] S. Bilgen, Structure and environmental impact of global energy consumption, Renew. Sustain. Energy Rev. 38 (2014) 890–902, https://doi.org/10.1016/j.rser.2014.07.004.

[39] A. Badreldin, O. Bouhali, A. Abdel-Wahab, Complimentary computational cues for water electrocatalysis: A DFT and ML perspective, Adv. Funct. Mater. 34 (2024), https://doi.org/10.1002/adfm.202312425.

[40] A. Rajabi, R. Grotjahn, D. Rappoport, F. Furche, A DFT perspective on organometallic lanthanide chemistry, Dalton Trans. 53 (2024) 410–417, https://doi.org/10.1039/D3DT03221C.

[41] N. Selmane, A. Cheknane, H.S. Hilal, Optimization of Al-doped ZnO transparent conducting oxide and emitter layers for enhanced performance of Si heterojunction solar cells, J Electron Mater 49 (2020) 2179–2190, https://doi.org/10.1007/s11664-019-07917-w.

[42] J. El Hamdaoui, M. El-Yadri, K. Lakaal, M. Kria, M. Courel, M. Ojeda, L.M. Pérez, D. Laroze, E. Feddi, Ab initio study on electronic and optical properties of Cu2NiGeS4 for photovoltaic applications, Solar Energy 237 (2022) 333–339, https://doi.org/10.1016/j.solener.2022.03.052.

[43] S.M.H. Qaid, A. Shaker, K. Deepthi Jayan, M. Alkadi, A. Ahmed Ali Ahmed, W. Zein, Design and numerical simulation of B-γ CsSnI3-based perovskite solar cells: conventional versus inverted configurations, Solar Energy 268 (2024) 112275, https://doi.org/10.1016/j.solener.2023.112275.

[44] M.A. Ullah, S.D. Shuvo, D.A. Roy, An attempt to improve the efficiency of CZTSSe solar cell using a P type Al-ga-Sb as a bi-layer material, SSRN Electron. J. (2024), https://doi.org/10.2139/ssrn.4977652.

[45] N. Selmane, A. Cheknane, H.S. Hilal, A new CsPbI2Br/CuZnSnSSe/Si tandem solar cell with higher than 32% efficiency, Micro and Nanostructures 194 (2024) 207940, https://doi.org/10.1016/j.micrna.2024.207940.

[46] Md. Ferdous Rahman, Md. Al Ijajul Islam, M. Chowdhury, L. Ben Farhat, S. Ezzine, A.T.M., Saiful Islam, efficiency improvement of CsSnI3 based heterojunction solar cells with P3HT HTL: A numerical simulation approach, Mater. Sci. Eng. B 307 (2024) 117524, https://doi.org/10.1016/j.mseb.2024.117524.

[47] H. Heriche, I. Bouchama, N. Bouarissa, Z. Rouabah, A. Dilmi, Enhanced efficiency of Cu(In,Ga)Se2 solar cells by adding Cu2ZnSn(S,Se)4 absorber layer, Optik (Stuttg) 144 (2017) 378–386, https://doi.org/10.1016/j.ijleo.2017.07.006.

[48] U. Saha, A. Biswas, Md.K. Alam, Efficiency enhancement of CZTSe solar cell using CdS(n)/(AgxCu1−x)2ZnSnSe4 (p) /Cu2ZnSnSe4 (p+) structure, Solar Energy 221 (2021) 314–322, https://doi.org/10.1016/j.solener.2021.04.043.

[49] M.F. Rahman, M.M. Ahmad, T.A. Chowdhury, S. Singha, Performance improvement of three terminal heterojunction bipolar transistor based hybrid solar cell using nano-rods, Sol. Energy 240 (2022) 1–12, https://doi.org/10.1016/j.solener.2022.05.006.

[50] N. Selmane, A. Cheknane, M. Aillerie, H.S. Hilal, Effect of ZnO-based TCO on the performance of a-Si H(n)/a-Si H(i)/c-Si H(p)/Al BSF(p+)/Al heterojunction solar cells, Environ. Prog. Sustain. Energy 38 (2019), https://doi.org/10.1002/ep.13114.

[51] M. Zhang, K. Chen, Y. Wei, W. Hu, Z. Cai, J. Zhu, Q. Ye, F. Ye, Z. Fang, L. Yang, Q. Liang, Strategies for optimizing the morphology of CsSnI3 perovskite solar cells, Crystals (Basel) 13 (2023) 410, https://doi.org/10.3390/cryst13030410.

[52] X. Zhang, D. Zhang, Z. Wang, Y. Zhao, H. Chen, All-inorganic tin-containing perovskite solar cells: an emerging eco-friendly photovoltaic technology, Adv. Mater. (2025), https://doi.org/10.1002/adma.202505543.